Int. J. Solids Structures Vol. 30, No. 13, pp. 1789–1806, 1993
Printed in Great Britain

0020–7683/93 $6.00+ .00
Pergamon Press Ltd

STICK–SLIP IN THE THIN FILM PEEL TEST—I. THE 90° PEEL TEST

K.-H. TSAI and K.-S. KIM
Division of Engineering, Brown University, Providence, RI 02912, U.S.A.

(*Received* 18 *June* 1992; *in revised form* 20 *October* 1992)

Abstract—An analysis of the process of stick–slip in the 90° peel test is carried out using a slender-elastic-beam theory which considers both stretching and bending of the film. Using an energy-based crack propagation criterion, it is shown that the intersection between the energy release rate curve and the interface toughness curve delineates the limit cycle on the interface toughness versus crack-growth rate plane for stick–slip 90° peeling. As a result of this analysis, it has been found that the effects of bending are significant and cannot be neglected in the general case. In addition, the stick–slip period and frequency have been found to depend on Young's modulus, and the thickness and length of the free film, and the dependence differs for the bending-dominant and stretching-dominant peel tests.

1. INTRODUCTION

The thin-film peel test is often used to measure adhesion strength (Kim and Kim, 1988; Kinloch and Yuen, 1989). Two different types of peel set-ups are commonly used; the L peel test, and the roller peel test. In the L peel test a strip of thin flexible film bonded to a flat substrate is peeled apart at some fixed angle to the underlying substrate as shown in Fig. 1(a). Generally, 90° peeling is preferred because it is relatively simple both experimentally and for theoretical analysis. In the roller peel test a thin strip of film bonded to a roller is peeled off as shown in Fig. 1(b). In this case the peel angle varies with time during the test. Stick–slip (or run–arrest) peeling is observed in both types of peel tests for certain ranges of peeling speed. The process of stick–slip observed in the thin-elastic-film L peel test is considered in this paper. An analysis of stick–slip in the roller peel test will be presented in a subsequent paper, Part II (Tsai and Kim, 1993).

Phenomena of an intermittent nature such as stick–slip (or run–arrest) are observed in many fracture and friction experiments. Examples of such observations in fracture-related experiments include the force fluctuation in thin film peel tests (Gardon, 1963; Aubrey *et al.*, 1969; Kim *et al.*, 1989), tearing of rubber (Greensmith and Thomas, 1955)

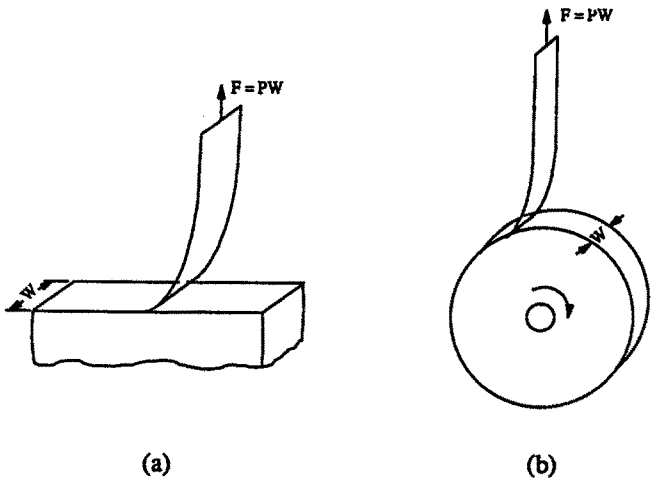

Fig. 1. Schematic representation of the peel tests.

and crack propagation in epoxy resin (Selby and Miller, 1975; Spanoudakis and Young, 1980). It has also been observed in friction-related experiments such as fiber pull-out (Cook *et al.*, 1989; Tsai and Kim, 1991), microscratch test (Wu, 1991), rock friction (Dieterich, 1979) and friction between two plates with some lubrication (Thompson and Robbins, 1990). This intermittent motion is created by a mechanism that generates cycles of crack-growth (or sliding) instability followed by subsequent arrest (or stabilization).

In this paper the stick–slip associated with crack-growth in the peel test is our main interest. The alternation between instability and stability in peeling is produced by the competition between the change in the driving force (or energy release rate) and the change in the crack-growth resistance (or toughness), associated with the crack growth. The frequency and amplitude (or run–arrest jumping distance) of the stick–slip process depends on the details of the mechanism of crack growth. The change in the driving force associated with crack growth depends on the specimen geometry, the loading history, the deformation characteristics of the specimen, and the inertia involved in the crack-growth process. On the other hand, the change in the resistance (toughness) depends on the crack-growth history. The history dependence results from the micro-mechanisms of the interface fracture process.

If the size of the fracture-process zone is very small compared to the smallest geometrical dimension of the specimen, and if the fracture process is a viscous phenomenon, the crack-growth history dependence of the toughness can be approximated as crack-growth rate dependence; then the interface toughness is simply a function of crack-growth rate. Some examples of the measurement of interface toughness as a function of crack-growth rate are reported for a scotch tape interface in Maugis and Barquins (1987), and for the interface between a pressure-sensitive adhesive tape and a glass substrate (Aubrey *et al.*, 1969). In this paper we denote the energy release rate as G, the interface toughness as $\mathscr{G}$ and the crack growth rate as $\dot{q}$. In general the interface toughness is known to be not only a function of crack-growth rate but also a function of crack-tip mode mixity (Liechti and Chai, 1992). However, the mode mixity in a peel test is insensitive to peel angle, and it is practically a fixed value unless the peeling occurs at a very shallow angle (Thouless and Jensen, 1992). Therefore we regard the interface toughness, $\mathscr{G}$, as a function of only the crack-growth rate, $\dot{q}$, for the peel analysis.

Analyses in later sections show that 90° elastic-peeling with constant peeling speed, v, generates unstable crack growth when $d\mathscr{G}/d\dot{q} < 0$, and it gives stable crack growth when $d\mathscr{G}/d\dot{q} > 0$. Once the instability is generated, stick–slip proceeds with the energy release rate, G, and the crack-growth rate, $\dot{q}$, tracing a closed path in the $(G, \dot{q})$ plane, with the time t parameterizing the loop. Then the state of peeling expressed in terms of the crack-growth rate, $\dot{q}$, and the peel force (per unit width), P, also traces a closed path in the $(P, \dot{q})$ plane. The closed path in the $(P, \dot{q})$ plane is called the "stick–slip limit cycle" (Maugis and Barquins, 1987). However, if the film is not elastic, or if the effects of inertia are significant in the peeling process as in the roller peel test, the trace of $(P, \dot{q})$ for the stick-slip process no longer follows the limit cycle; instead it makes a complicated trajectory in the $(P, \dot{q})$ plane (Maugis and Barquins, 1987).

In general, the stick–slip in the 90° peel test of constant speed peeling results in periodic fluctuations in the peel force, and the observed frequency of the stick–slip in the 90° peel test is lower than that seen in the roller peel test. The roller peel test sometimes generates chaotic stick–slip motions for a certain range of the peeling speed (Maugis and Barquins, 1987). In the 90° peel test, it is observed that if the deformation of the film is elastic the amplitude of the peel force fluctuation due to stick–slip does not depend on the thickness of the film or the speed of peeling; while plastic deformation of the film results in an amplitude variation with film thickness. Kim and Kim (1988) reported that, for a 90° peel test of thin copper films on a silicon substrate, the amplitude and wave length of the stick–slip fluctuation increase as film thickness decreases. However, a consideration of plasticity is beyond the scope of this paper; the relationship between elastic behavior of the film and the rate-dependent behavior of the interface toughness is the main interest.

Several investigators have proposed models of the stick–slip process to predict the dependence of stick–slip frequency on the peeling speed, and the length, thickness and

elastic properties of the film. Maguis and Barquins (1987) studied the process of stick–slip for both the 90° and the roller peel tests with the film considered to be elastic. Webb and Aifantis (1989) analysed the 90° peel test for a viscoelastic film. However, these models only considered pure stretching of the film; the effects of bending were neglected. This paper addresses modeling the film deformation in stick–slip peeling, including both bending and stretching. The results of the analysis show that the effects of bending cannot, in general, be neglected. The results show opposite trends in the variation of frequency with the thickness and elastic stiffness of the film for stretching-dominant and bending-dominant peeling processes. The bending effect is even more important in predicting the stick–slip frequencies in the roller peel test, the modeling of which is presented in a subsequent paper, Part II (Tsai and Kim, 1993).

Mathematical formulation of the stick–slip problem for 90° elastic peeling is described in Section 2. In 2.1, energy balance in quasi-static elastic peeling is considered. Then, in 2.2, the energy balance equation is connected with the detailed analysis of the bending and stretching film-deformation to derive the equation of crack growth for 90° peeling. This crack-growth equation is used to analyse the stick–slip cycle for 90° peeling in 2.3. The governing equation is a first order nonlinear ordinary differential equation for the crack-growth rate as a function of time, and solutions are obtained through numerical analysis. To solve the equation a specific relationship between the interface toughness and the crack-growth rate is required; in the analysis the experimental relationship for a scotch-tape adhesive reported by Maugis and Barquins (1987) was used. The numerical results are reported in Section 3. The stick–slip frequency as a function of the peeling speed, the thickness of the film and the stiffness of the film is presented in 3.1. In 3.2, detailed numerical results of the stick–slip process are presented for bending- and stretching-dominant peelings. Then discussion and conclusion follow in Sections 4 and 5, respectively.

2. FORMULATION OF THE PROBLEM

2.1. *Energy balance*

A schematic diagram of the peel test is shown in Fig. 2. The adherend is assumed to be elastic for the stick–slip analysis. If global plastic deformation is excluded, the work done by the peel force is partly stored as the energy of elastic deformation in the film, and the rest is consumed in the local fracture process to create the new fracture surfaces. In this case, neglecting the inertia of the film, the J integral around the crack tip yields the energy release rate G. Furthermore, from path independence of the J integral, the energy release rate G can be equated to the J integral at the far field which is expressed as [Kim and Kim (1988); this expression of energy balance was also used by others earlier, e.g. Kendall (1975)]

$$G = (1-\cos\phi)P + \frac{P^2}{2Eh}, \tag{1}$$

where P is the peel force per unit width of the film, ϕ is the peel angle, $E = E_0$ for the plane

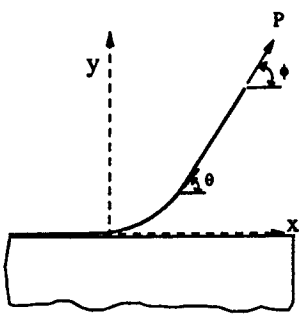

Fig. 2. Schematic diagram of peeling.

stress case and $E = E_0/(1-\nu^2)$ for the plane strain case, E_0 and ν are the Young's modulus and Poisson's ratio of the film, and h is the thickness of the film. The energy-based crack-propagation criterion employed in this analysis is that the interface crack propagates only if the energy release rate, G, reaches the value of the interface toughness, $\mathcal{G}$. In the peel test of a viscoelastic adhesive such as scotch tape, the interface toughness, $\mathcal{G}$, is a function of the peeling rate, $\dot{q}$, because of the viscoelastic deformation of the adhesive. Therefore, during a stick–slip peeling process, the energy release rate, G, fluctuating as a cyclic curve is traced out in the $(G, \dot{q})$ plane. The cyclic curve is the trace of the intersection points between the toughness, $\mathcal{G}(\dot{q})$, and the admissible energy release rate, $G(\dot{q}; P)$. Equation (1) shows that the energy release rate, G, is not a function of $\dot{q}$; it is a constant for given values of the peel force, P, and the peel angle, ϕ. As will be seen later, only in such cases does the cyclic curve in the $(G, \dot{q})$ plane become the limit cycle used by Maugis and Barquins (1987).

2.2. *Analysis of crack growth in 90° peeling*

For the analysis of stick–slip peeling, a quasistatic slender beam theory that considers both bending and stretching is used to model the deformation of the film. As shown in Fig. 2 the origin of the x and y coordinates is fixed at the crack tip of the interface. The governing equations of equilibrium and moment balance are [see also Kim and Kim (1988)]

$$\frac{dT}{ds} - KN = 0, \tag{2a}$$

$$\frac{dN}{ds} + KT = 0, \tag{2b}$$

$$\frac{dM}{ds} + N = 0, \tag{2c}$$

where T and N are the axial and shear forces per unit width of the film, $K = d\theta/ds$ is the curvature of the neutral axis of the film, $\tan\theta$ is the slope of the neutral axis of the film, M is the bending moment per unit width of the film, and s is the arc length along the neutral axis of the stretched film.

From overall equilibrium of the film the axial force, T, and the shear force, N, can be expressed as

$$T = P\cos(\phi - \theta), \tag{3a}$$

$$N = P\sin(\phi - \theta). \tag{3b}$$

Substituting the relations of eqns (3) into eqns (2), the equilibrium equations (2a) and (2b) are automatically satisfied and the remaining moment equation (2c) becomes

$$\frac{dM}{ds} + P\sin(\phi - \theta) = 0. \tag{4}$$

The coordinate axes and sign conventions are indicated in Fig. 3 for a film subjected to a pure bending moment M. According to this figure the bending moment is expressed as $M = EIK$, where $I\ (=h^3/12)$ is the moment of inertia of the cross-section about the z-axis per unit width of the film. Substituting the expression of the bending moment, M, into eqn (4), it becomes

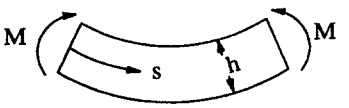

Fig. 3. Slender beam under pure bending.

$$EI\frac{dK}{d\theta}\frac{d\theta}{ds}+P\sin(\phi-\theta)=0. \tag{5}$$

Since $d\theta/ds = K$, eqn (5) is a first-order nonlinear differential equation for $K(\theta)$. The bending curvature K can be integrated with the boundary condition, $K = 0$ at $\theta = \phi$, to give the relationship,

$$K=\frac{2}{h}\{6\bar{P}[1-\cos(\phi-\theta)]\}^{1/2}, \tag{6}$$

where $\bar{P} = P/Eh$. In the following derivations the length is normalized with the thickness h, and the normalization will be indicated by $\bar{}$. In addition, only 90° peeling will be considered in this paper, i.e. $\phi = \pi/2$. In this case K becomes

$$K=\frac{2}{h}[6\bar{P}(1-\sin\theta)]^{1/2}. \tag{7}$$

From eqn (7) the normalized arc length $\bar{s}$ can be integrated as a function of θ with the boundary condition, $\bar{s} = 0$ at $\theta = 0$:

$$\bar{s}=\tfrac{1}{4}(3\bar{P})^{-1/2}\left[\ln\frac{\sqrt{1+\sin\theta}+\sqrt{2}}{(-\sqrt{1+\sin\theta}+\sqrt{2})(3+2\sqrt{2})}\right]. \tag{8}$$

This equation shows that the slope angle, θ, approaches $\pi/2$ asymptotically with $\bar{s}$ approaching infinity. This indicates that the arc length is required to be infinite to have 90° peeling unless a bending moment is applied at a finite end of the film. However, we assume that essentially 90° peeling conditions are achieved if the length of the film is longer than the length, $\bar{s}_f$, corresponding to a slope angle, θ, very close to 90°, say 89.9° in eqn (8). In other words, a vertical loading applied at the end of the film of length, $\bar{s}_0$, makes the peel configuration approximately 90°, if the following condition is satisfied:

$$\bar{s}_0 \geqslant \bar{s}_f = 1.98\bar{P}^{-1/2}. \tag{9}$$

Integrating $d\bar{y} = \sin\theta\, d\bar{s}$ with eqn (8), we have the relationship,

$$\bar{y}=(6\bar{P})^{-1/2}\left\{1-\sqrt{2}\frac{\mathscr{A}-1}{\mathscr{A}+1}\right\}+\bar{s}, \tag{10a}$$

$$\mathscr{A}=(3+2\sqrt{2})\exp(4\sqrt{3\bar{P}}\bar{s}). \tag{10b}$$

Now we are interested in expressing the vertical position of the material point, $\bar{y}$, in terms of the undeformed-configurational length, $\bar{S}$, instead of the deformed length, $\bar{s}$. The deformed arc length, $\bar{s}$, is then decomposed as

$$\begin{aligned}\bar{s}&=\bar{S}+\int_0^S \varepsilon\, d\bar{S}\\ &=\bar{S}+\int_0^{\bar{s}}\varepsilon\frac{d\bar{s}}{1+\varepsilon},\end{aligned} \tag{11}$$

where ε is the strain due to stretching along the arc length direction. Neglecting the second order term of ε, $\bar{s}$ can be expressed as

$$\bar{s} = \bar{S} + \int_0^{\bar{s}} \varepsilon \, d\bar{s} + O(\varepsilon_0^2 \bar{S})$$

$$= \bar{S} + \bar{P} \int_0^{\bar{s}} \sin\theta \, d\bar{s} + O(\varepsilon_0^2 \bar{S})$$

$$= \bar{S} + \bar{P}\bar{y} + O(\varepsilon_0^2 \bar{S}), \tag{12}$$

where ε_0 is the stretching strain of the film near the loading point; $\varepsilon_0 = \bar{P}$. Then, substituting eqn (12) into eqns (10), we have

$$\bar{y} = (1-\bar{P})^{-1} \left\{ (6\bar{P})^{-1/2} \left[1 - \sqrt{2} \frac{\mathscr{A}-1}{\mathscr{A}+1} \right] + \bar{S} \right\} + O(\varepsilon_0^2 \bar{S}), \tag{13a}$$

$$\mathscr{A} = (3+2\sqrt{2}) \exp\{4\sqrt{3\bar{P}}(\bar{S}+\bar{P}\bar{y})\}. \tag{13b}$$

Considering y and S as the height and the undeformed-configurational arc length at the loading point, the time derivative of y represents the peeling speed v at the loading point, which is a constant in the constant-speed peel test. The arc length change rate, $\dot{S}$, is identical to the crack-growth rate $\dot{q}$ which is the crack propagation speed at the interface. In the following, all the symbols related to the crack-growth rate $\dot{q}$ will be, therefore, replaced by the corresponding symbols related to the arc length change rate $\dot{S}$. Taking the time derivative of eqns (13), we have the relationship,

$$\left\{ \frac{1}{2\sqrt{6}} \bar{P}^{-3/2} \left[\sqrt{2} \frac{\mathscr{A}-1}{\mathscr{A}+1} - 1 \right] + \bar{y} \left[1 - \frac{12\mathscr{A}}{(\mathscr{A}+1)^2} \right] - \frac{4\mathscr{A}}{(\mathscr{A}+1)^2} \frac{\bar{S}}{\bar{P}} + O(\varepsilon_0 \bar{S}) \right\} \frac{d\bar{P}}{d\bar{t}}$$

$$+ \left\{ 1 - \frac{8\mathscr{A}}{(\mathscr{A}+1)^2} \right\} \hat{\dot{S}} + \left\{ \bar{P} \left[1 - \frac{8\mathscr{A}}{(\mathscr{A}+1)^2} \right] - 1 \right\} \hat{v} = O(\varepsilon_0^2 \hat{\dot{S}}), \tag{14}$$

where $\bar{t} = t\dot{S}_C/h$; $\dot{S}_C$ is the characteristic crack-growth rate at which the interface toughness has local maximum $\mathscr{G}_C$, and $\hat{}$ indicates normalization with respect to the characteristic crack-growth rate, $\dot{S}_C$.

From eqn (1) the normalized peel force, $\bar{P}$, for the 90° peel test can be expressed as

$$\bar{P} = \sqrt{1 + 2\bar{\mathscr{G}}_C \hat{G}} - 1, \tag{15}$$

where $\bar{\mathscr{G}}_C = \mathscr{G}_C/Eh$ and $\hat{G} = G/\mathscr{G}_C$. As indicated previously, $G = \mathscr{G}$ during peeling, and $\mathscr{G}$ is a function of the crack-growth rate, $\dot{S}$. Therefore, the variation of peel force with time can be derived as

$$\frac{d\bar{P}}{d\bar{t}} = \frac{\bar{\mathscr{G}}_C \hat{\mathscr{G}}'}{\sqrt{1 + 2\bar{\mathscr{G}}_C \hat{\mathscr{G}}}} \frac{d\hat{\dot{S}}}{d\bar{t}}, \tag{16}$$

where $'$ represents the first derivative with respect to the normalized crack-growth rate $\hat{\dot{S}}$.

Substituting eqns (13), (15) and (16) into eqn (14) yields the governing equation of crack growth for 90° stick–slip peeling. However, further simplification of the crack-growth equation is possible because $\mathscr{A}$ in eqn (13b) is an exceptionally large number for the requirement of 90° peel configuration. The requirement, $\bar{s} \geqslant \bar{s}_f$ for $\bar{s} = \bar{s}_0$, in eqn (9) is then rendered as

$$\mathscr{A} \geqslant \mathscr{A}_f = (3+2\sqrt{2}) \exp(4\sqrt{3\bar{P}\bar{s}_f})$$

$$= 5.25 \times 10^6. \tag{17}$$

Since $\mathscr{A}_f$ is such a large number, and $\mathscr{A}$ is even larger, the following approximations can be used:

$$\frac{\mathscr{A}-1}{\mathscr{A}+1} = 1+O\left(\frac{1}{\mathscr{A}}\right), \tag{18a}$$

$$\frac{\mathscr{A}}{(\mathscr{A}+1)^2} = \frac{1}{\mathscr{A}}\left\{1+O\left(\frac{1}{\mathscr{A}}\right)\right\}, \tag{18b}$$

$$\bar{y} = (1-\bar{P})^{-1}\left\{(6\bar{P})^{-1/2}\left[1-\sqrt{2}+O\left(\frac{1}{\mathscr{A}}\right)\right]+\bar{S}\right\}+O(\varepsilon_0^2\bar{S}). \tag{18c}$$

By applying these approximations, eqn (14) is reduced to give the explicit governing equation of crack growth in 90° peeling:

$$\left\{\frac{\sqrt{2}-1}{2\sqrt{6}}\left(\frac{4-3\sqrt{1+2\bar{\mathscr{G}}_C\hat{\mathscr{G}}}}{2-\sqrt{1+2\bar{\mathscr{G}}_C\hat{\mathscr{G}}}}\right)(\sqrt{1+2\bar{\mathscr{G}}_C\hat{\mathscr{G}}}-1)^{-3/2}+\bar{S}+O(\varepsilon_0\bar{S})+O\left(\frac{\varepsilon_0^{-3/2}}{\mathscr{A}}\right)\right\}\bar{\mathscr{G}}_C\hat{\mathscr{G}}'\frac{d\hat{S}}{d\bar{t}}$$
$$+\hat{S}-(2-\sqrt{1+2\bar{\mathscr{G}}_C\hat{\mathscr{G}}})\hat{v} = O(\varepsilon_0^2\hat{S})+O\left(\frac{\hat{S}}{\mathscr{A}}\right)+O\left(\frac{\varepsilon_0\hat{v}}{\mathscr{A}}\right). \tag{19}$$

Now, neglecting the higher order terms, eqn (19) is expressed as

$$(F_b+F_s)\hat{\mathscr{G}}'\frac{d\hat{S}}{d\bar{t}}+\hat{S}-(1-\varepsilon_0)\hat{v} = 0, \tag{20a}$$

where F_b and F_s are terms representing bending and stretching contributions, and they are given by

$$F_b = \frac{\sqrt{2}-1}{2\sqrt{6}}\left(\frac{4-3\sqrt{1+2\bar{\mathscr{G}}_C\hat{\mathscr{G}}}}{2-\sqrt{1+2\bar{\mathscr{G}}_C\hat{\mathscr{G}}}}\right)(\sqrt{1+2\bar{\mathscr{G}}_C\hat{\mathscr{G}}}-1)^{-3/2}\bar{\mathscr{G}}_C$$
$$\approx \frac{\sqrt{2}-1}{2\sqrt{6}}\bar{\mathscr{G}}_C^{-1/2}\hat{\mathscr{G}}^{-3/2} \quad \text{for } \bar{\mathscr{G}}_C\hat{\mathscr{G}} \approx \bar{P} \ll 1, \tag{20b}$$

$$F_s = \bar{\mathscr{G}}_C\bar{S}. \tag{20c}$$

Equations (20) are the reduced equations of crack growth for 90° peeling with small stretching-strain and long detached length of film.

If we neglect the bending effect, then $\bar{y} = \bar{s}$ in eqn (10a), and the subsequent derivation for eqns (20) shows that $F_b = 0$. On the other hand, if we assume that the film is almost inextensible, then $\bar{s} \approx \bar{S}$ in eqns (10), and the subsequent derivation for eqns (20) yields that F_s is negligible compared to F_b. Therefore we see that the F_b term results from the bending of the film, while the F_s term results from the stretching of the film. Accordingly, the peeling is bending dominant if $F_b \gg F_s$, and stretching dominant if $F_b \ll F_s$. Or in terms of $\bar{P}$ and $\bar{S}$, if $\bar{P}^{-3/2} \gg 11.8\bar{S}$ then it is bending-dominant peeling, and if $\bar{P}^{-3/2} \ll 11.8\bar{S}$, it is stretching-dominant peeling. In some analyses (Maugis and Barquins, 1987; Webb and Aifantis, 1989) only the stretching term was considered; the effects of bending were neglected. This assumption introduces a significant error for most peeling situations. For example, if we consider the peeling of 100 μm thick glassy polymeric film with a Young's modulus of 3 GPa and an adhesion strength of 120 J m^{-2}, the bending contribution, F_b, and the stretching contribution, F_s, are comparable if the detached length of the film is equal to 1 m. In this case, therefore, the detached film length should be much longer than 1 m in order to neglect the bending term. The assumption of stretching-dominant peelings

becomes worse if the adhesion strength is weak; if the adhesion strength is 12 J m^{-2}, the film must be much longer than 30 m to have stretching-dominant peeling.

Now let us examine eqns (20) a little closer. For constant speed peeling one of the solutions of eqns (20) is $\hat{S} = (1-\varepsilon_0)\hat{v}$. This solution implies $d\hat{S}/d\bar{t} = 0$, and therefore it is the steady-state solution. In addition, the stability of this steady-state solution can be examined with eqns (20). If we consider a small perturbation $\delta = \hat{S} - (1-\varepsilon_0)\hat{v}$ at time $\bar{t}_0$, in which $\delta/\hat{S} \ll 1$, then the solution becomes

$$\hat{S} - (1-\varepsilon_0)\hat{v} \approx \delta \exp\{-[(F_b+F_s)\hat{\mathscr{G}}'(\hat{S}(\bar{t}_0))]^{-1}(\bar{t}-\bar{t}_0)\} \quad \text{for small } \bar{t}-\bar{t}_0. \tag{21}$$

In eqn (21) the term $F_b + F_s$ is always positive, and therefore the sign of $\hat{\mathscr{G}}'$ determines the stability. If $\hat{\mathscr{G}}'$ is positive, the perturbation decays with time, and the steady-state solution is stable; while if $\hat{\mathscr{G}}'$ is negative, the steady-state solution is unstable.

2.3. *Analysis of a stick–slip cycle*

In this section we examine how the equations of crack growth, eqn (19) or eqns (20), can describe the stick–slip process and provide values for the stick–slip frequencies. As mentioned in the introduction, we are modeling the stick–slip process caused by the interaction between the elastic deformation of the thin film and the rate-dependent resistance, $\hat{\mathscr{G}}(\hat{S})$, of the crack growth in the peeling process. Therefore we are employing a particular type of crack-growth resistance, $\hat{\mathscr{G}}(\hat{S})$, for our discussion. The crack-growth resistance, $\hat{\mathscr{G}}(\hat{S})$, which is also called the interface toughness, has a typical form for viscoelastic adhesives as shown in Fig. 4, as reported by Maugis and Barquins (1987) for scotch tape. It has two distinct regions *ABC* and *FED* for which $\hat{\mathscr{G}}' > 0$, and region *CF* for which $\hat{\mathscr{G}}' < 0$, as indicated in the figure. As we have described in the previous section, if the peeling speed is imposed in the range of $(1-\varepsilon_0)\hat{v} < \hat{S}_C$ or $\hat{S}_F < (1-\varepsilon_0)\hat{v}$, in which $\hat{\mathscr{G}}' > 0$, then $\hat{S} = (1-\varepsilon_0)\hat{v}$ is the stable steady-state solution. However, if the peeling speed is in the range of $\hat{S}_C < (1-\varepsilon_0)\hat{v} < \hat{S}_F$, in which $\hat{\mathscr{G}}' < 0$, then there cannot be a stable steady-state solution. Therefore the curve *CF* in Fig. 4 is called the unstable branch. Provided that $\hat{\mathscr{G}}' \neq 0$, eqn (20a) can be rearranged as follows:

$$\frac{d\hat{S}}{d\bar{t}} = -\frac{\hat{S}-(1-\varepsilon_0)\hat{v}}{(F_b+F_s)\hat{\mathscr{G}}'}. \tag{22}$$

When the peeling speed is set in the range of $\hat{S}_C < (1-\varepsilon_0)\hat{v} < \hat{S}_F$, the sign of $d\hat{S}/d\bar{t}$ in

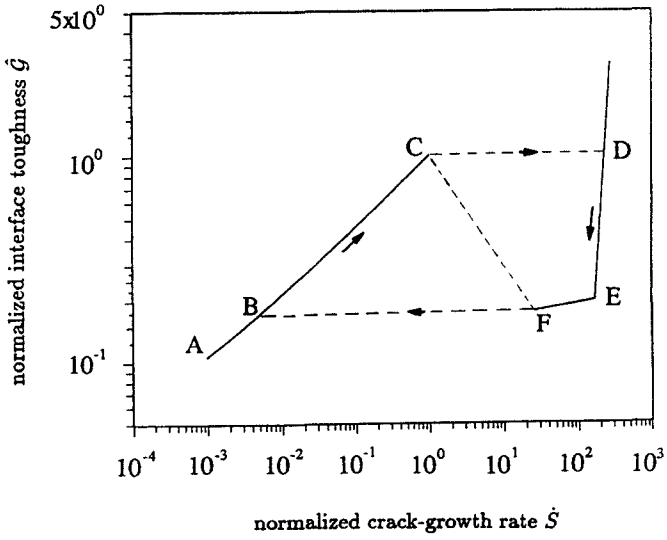

Fig. 4. The interface toughness $\hat{\mathscr{G}}(\hat{S})$ curve. $\hat{S} = \dot{S}/\dot{S}_C$; $\dot{S}_C = 7.96\times10^{-2}$ m s^{-1} and $\hat{\mathscr{G}} = \mathscr{G}/\mathscr{G}_C$; $\mathscr{G} = 170.0$ J m^{-2}.

eqn (22) shows that any crack-growth rate, $\hat{S}$, in the range of $\hat{S} < (1-\varepsilon_0)\hat{v}$ tends to move towards $\hat{S}_C$, and that in the range of $\hat{S} < (1-\varepsilon_0)\hat{v}$ towards $\hat{S}_F$. Once the peeling state $(\hat{S}, \hat{G})$ reaches the critical point C or F, it must jump to another admissible branch of $(\hat{S}, \hat{\mathscr{G}})$. In other words if the peeling state $(\hat{S}, \hat{G})$ starts to follow the $(\hat{S}, \hat{\mathscr{G}})$ branch of ABC, the peeling state moves towards the state at C. Once it reaches the state at C, it jumps to the next stable branch DEF. As it approaches C, $\hat{\mathscr{G}}'$ approaches 0^+ and consequently $d\hat{S}/d\bar{t}$ approaches infinity, indicating an instantaneous jump from the crack-growth rate $\hat{S}_C$ to $\hat{S}_D$. At the instant of the jump the peel force, $\bar{P}$, is only a function of peeled-film configuration; it is independent of the instantaneous crack-growth rate. Consequently the energy release rate, $\hat{G}$, which is a function of the peel force, $\bar{P}$ [eqn (15)], does not change as the crack-growth rate jumps. This indicates that it has to be a horizontal jump in Fig. 4; it jumps from C to D in the figure. Once it jumps to point D, the peeling state is on the branch of DEF and the crack-growth rate $\hat{S}$ is in the range of $\hat{S} > (1-\varepsilon_0)\hat{v}$. Then the peeling state starts to move towards point F, following the curve DEF in Fig. 4. When the peeling state reaches point F, it undergoes a jump to the state B in Fig. 4, analogous to the jump from state C to state D. As the peeling state re-enters the $(\hat{S}, \hat{\mathscr{G}})$ branch of ABC, it repeats the above-mentioned processes. As a result, the peeling state $(\hat{S}, \hat{G})$ forms a limit cycle $BCDEF$, and stick–slip occurs as $\hat{G}$ and $\hat{S}$ fluctuation along this limit cycle. The period of the stick–slip cycle, therefore, should correspond to the time spent on both the BC and DEF regions.

From eqn (20a), neglecting the ε_0 term, the stick–slip period can be integrated as follows:

$$\Delta\bar{t} = \int_{\hat{\mathscr{G}}_B}^{\hat{\mathscr{G}}_C} \frac{F_b + F_s}{\hat{v} - \hat{S}(\hat{\mathscr{G}})}\, d\hat{\mathscr{G}} + \int_{\hat{\mathscr{G}}_D}^{\hat{\mathscr{G}}_F} \frac{F_b + F_s}{\hat{v} - \hat{S}(\hat{\mathscr{G}})}\, d\hat{\mathscr{G}}, \tag{23}$$

where $\hat{\mathscr{G}}_C = \hat{\mathscr{G}}_D = 1$, the crack-growth rate, $\hat{S}$, in the first integral is a function of the toughness, $\hat{\mathscr{G}}$, along the curve BC, and in the second the crack-growth rate is a function of the toughness integral along the curve DEF. The period can be separated into two terms; one is Δt_b which is due to the bending effect, F_b, and the other is Δt_s due to the stretching effect, F_s. Though the arc length S appears to be a function of F_s in eqn (20c), it will be treated as a constant in the integral of eqn (23) because its variation during one stick–slip cycle is very small compared to S itself. Therefore the period of one stick–slip cycle is expressed as

$$\Delta t = \Delta t_b + \Delta t_s, \tag{24a}$$

where

$$\Delta t_b = \dot{S}_C^{-1} \mathscr{G}_C^{-1/2} E^{1/2} h^{3/2} f_b(\hat{v}), \tag{24b}$$

$$\Delta t_s = \dot{S}_C^{-1} \mathscr{G}_C E^{-1} h^{-1} S f_s(\hat{v}), \tag{24c}$$

in which

$$f_b(\hat{v}) = \frac{\sqrt{2}-1}{2\sqrt{6}} \left(\int_{\hat{\mathscr{G}}_B}^{1} \frac{\hat{\mathscr{G}}^{-3/2}}{\hat{v} - \hat{S}(\hat{\mathscr{G}})}\, d\hat{\mathscr{G}} + \int_{1}^{\hat{\mathscr{G}}_F} \frac{\hat{\mathscr{G}}^{-3/2}}{\hat{v} - \hat{S}(\hat{\mathscr{G}})}\, d\hat{\mathscr{G}} \right), \tag{24d}$$

$$f_s(\hat{v}) = \int_{\hat{\mathscr{G}}_B}^{1} \frac{1}{\hat{v} - \hat{S}(\hat{\mathscr{G}})}\, d\hat{\mathscr{G}} + \int_{1}^{\hat{\mathscr{G}}_F} \frac{1}{\hat{v} - \hat{S}(\hat{\mathscr{G}})}\, d\hat{\mathscr{G}}. \tag{24e}$$

From eqns (24) we see that Δt_b is proportional to $E^{1/2}h^{3/2}$, and Δt_s is proportional to S but inversely proportional to Eh. Thus, if F_b is much larger than F_s in the bending-dominant peeling, the stick–slip period of the cycle is longer for stiffer and thicker films, and it is independent of the length of the film. On the other hand, if the stretching effect

dominates, i.e. F_s is much larger than F_b, then the trends are opposite to those of the bending-dominant case, and the period is longer for longer films.

3. NUMERICAL RESULTS

In this section we analyse numerically eqns (20) and (24) using the material constant and the function of $\hat{\mathcal{G}}$ given in Maugis and Barquins (1987). The Young's modulus E_0 of the scotch tape is given as 2.15 GPa. Here we consider the plane stress case, i.e. $E = E_0$. The explicit functions of the experimental curves along ABC and DE in Fig. 4 are also given by Maugis and Barquins (1987). Since the function of the curve EF is not given, we have selected a function to fit their experimental data. These functions are expressed as follows:

$$\hat{\mathcal{G}} = 0.0176(1+55.67\hat{S}^{0.35}) \quad \text{for } \hat{S}_B < \hat{S} < 1, \tag{25a}$$

$$\hat{\mathcal{G}} = \left(\frac{\hat{S}}{226.13}\right)^{5.5} \quad \text{for } \hat{S}_E < \hat{S} < \hat{S}_D, \tag{25b}$$

$$\hat{\mathcal{G}} = 0.176\left(\frac{\hat{S}}{26.38}\right)^{0.064} \quad \text{for } \hat{S}_F < \hat{S} < \hat{S}_E. \tag{25c}$$

The normalized crack-growth rate at B, C, D, E and F points are given as $\hat{S}_B = 5.47\times10^{-3}$, $\hat{S}_C = 1.0$, $\hat{S}_D = 226.13$, $\hat{S}_E = 168.57$ and $\hat{S}_F = 26.38$. The normalizing values for the toughness, $\mathcal{G}_C$, and for the crack-growth rate, $\dot{S}_C$, are provided as 170.0 J m^{-2} and 7.96×10^{-2} m s^{-1}, respectively.

3.1. *Stick–slip periods and frequencies*

Using the equations given in eqns (24), f_b and f_s are calculated, and they are plotted with respect to the peeling speed, $\hat{v}$, in Fig. 5. This figure shows that both f_b and f_s are approximately inversely proportional to the peeling speed, $\hat{v}$. As a consequence, from eqns (24), the stick–slip period Δt should have the same trend, and the stick–slip frequency is approximately proportional to the peeling speed, $\hat{v}$.

In order to compare the contributions to the period due to bending and stretching terms, a plot of Δt_b and Δt_s as a function of the film length S is shown in Figs 6(a) and

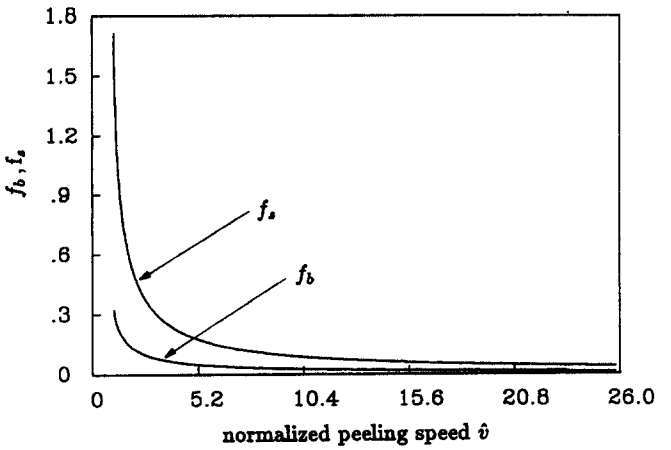

Fig. 5. Plot of f_b and f_s with respect to $\hat{v}$, respectively.

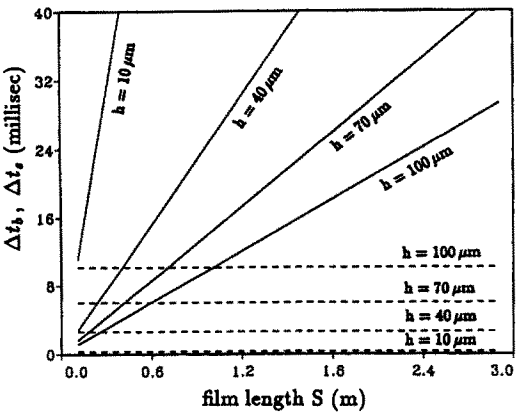

Fig. 6(a). Plot of Δt_b and Δt_s vs S, respectively, for $v = 0.1$ m s^{-1}. Δt_b : dotted line; Δt_s : solid line.

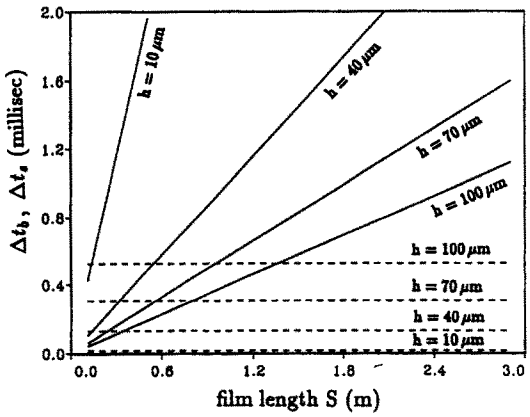

Fig. 6(b). Plot of Δt_b and Δt_s vs S, respectively, for $v = 2.0$ m s^{-1}. Δt_b : dotted line; Δt_s : solid line.

6(b). The contribution to the periods due to bending, Δt_b, are plotted with dotted lines in both figures, which are independent of the film length, S. In contrast, the contribution to the periods due to stretching, Δt_s, are plotted with solid lines, which are linearly proportional to the film length, S. Figure 6(a) is plotted for the case of low peeling speed [$v = 0.1$ m s^{-1} ($\hat{v} = 1.26$)], and Fig. 6(b) of high peeling speed [$v = 2.0$ m s^{-1} ($\hat{v} = 25.13$)]. In each figure the results for film thicknesses of 10, 40, 70 and 100 μm are plotted, and the thicknesses are indicated on the figures. The required minimum film length for the 90° peel configuration, s_f, for this scotch-tape peel test is of the order of 1 cm. Therefore, we have considered the film length longer than 10 cm for the plots in Figs 6(a) and 6(b). In both figures we see that 10 cm long and 40 μm thick tape has almost equal contributions for the stick–slip period from bending and stretching effects. Thus, the influence of bending cannot be neglected for a film length of this order. If the film length is as long as 2 m, the contribution of the bending effect to the total period of the stick–slip cycle is about 5%. Figures 6(a) and 6(b) also indicate that the influence of bending is more pronounced for thicker films. Furthermore, comparing the results in Figs 6(a) and 6(b), it is found that the bending effect becomes even more important at higher peeling speeds.

The stick–slip frequency can be obtained by determining the inverse of the period in eqns (24). The frequency is calculated for a film thickness of 40 μm, and plotted with respect to the peeling speed in Fig. 7 for four different film lengths: 0.1, 0.5, 1 and 3 m. This figure shows that the frequency is approximately proportional to peeling speed for longer films, for which the stretching effect is more dominant. On the other hand, if the film is shorter,

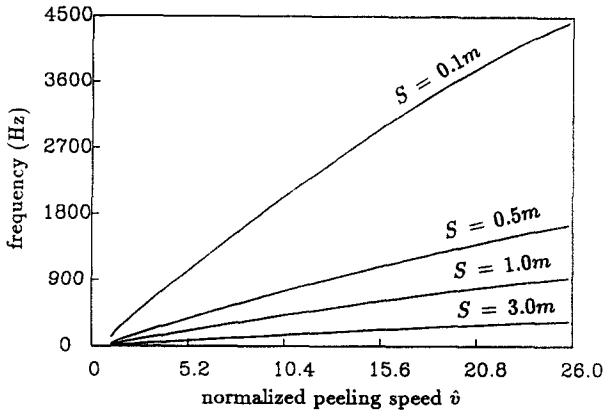

Fig. 7. Plot of stick–slip frequency vs normalized peeling speed $\hat{v}$. Thickness of the film is 40 μm, and the peeling speed is normalized with $\hat{S}_C$ ($=7.96\times10^{-2}$ m s^{-1}).

and the bending effect is more important, the frequency increases with the peeling speed, but the rate of increase decreases gradually with peeling speed.

3.2. *Comparison between bending- and stretching-dominant peelings*

In this section we compare the solutions of eqns (20) for the stick–slip processes of two extreme cases. One is the bending-dominant peeling, and the other is the stretching-dominant peeling. The length and thickness of the film are chosen to be 0.1 m and 100 μm respectively for the bending-dominant case, and 3 m and 10 μm respectively, for the stretching-dominant case. The stick–slip process in both low-speed peeling ($v = 0.1$ m s^{-1}) and high-speed peeling ($v = 2.0$ m s^{-1}) are analysed for each extreme case.

The peel force variations as a function of time are plotted in Fig. 8 for (a) bending-dominant low-speed peeling, (b) bending-dominant high-speed peeling, (c) stretching-dominant low-speed peeling, and (d) stretching-dominant high-speed peeling. From these figures, it is seen that the variation of the peel force is different for the bending- and stretching-dominant peelings, and for different peeling speeds as well. In bending-dominant low-speed peeling, initially the peel force increases slowly, then rapidly increases, as shown in Fig. 8(a). On the other hand, in stretching-dominant low-speed peeling, initially the peel force builds up rapidly, then increases more gradually, as shown in Fig. 8(c). Nevertheless, when the peel forces reach their maximum value, in both cases they drop suddenly to their lowest values. The shape of the peel force variation becomes sharp like a saw tooth, for high-speed peeling, for both cases as shown in Figs 8(b) and (d). However, the shape for the bending-dominant case has a cusp-like edge, as shown in Fig. 8(b), and the stretching-dominant one has a straight-kink edge, as shown in Fig. 8(d). It is interesting to note that plots similar to those shown in Figs 8(a) and (b) for the bending-dominant peeling were observed in the experimental results of Gardon (1963), who recorded the variation in peel force with time during a peel test of two cellophane films bonded with acrylic polymer Rhoplex B-60. On the other hand, the plots of the peel force variation with time shown in Figs 8(c) and (d) for the stretching-dominant peeling are similar to the results of Aubrey *et al.* (1969). In that study, peel tests were carried out with polyester films and glass substrates, and poly(*n*-butyl acrylate) was the adhesive.

The crack-growth rate, $\hat{S}$, is plotted as a function of time in Fig. 9. The displaying order (a), (b), (c) and (d) in Fig. 9 corresponds to those of Fig. 8. These figures show that at low peeling speed almost all the time is spent at the low crack-growth rate region, i.e. curve *BC* on the $\hat{\mathcal{G}}$ versus $\hat{S}$ graph in Fig. 4. However, the portion of time spent at high crack-growth rate range, curve *DEF*, increases with increasing peeling speed. Maugis and Barquins (1987) considered only the stretching effect in their relaxation oscillation model and calculated the period by neglecting the time spent on the high crack-growth rate branch. That approximation can be applied only to the peeling with a long film length and low

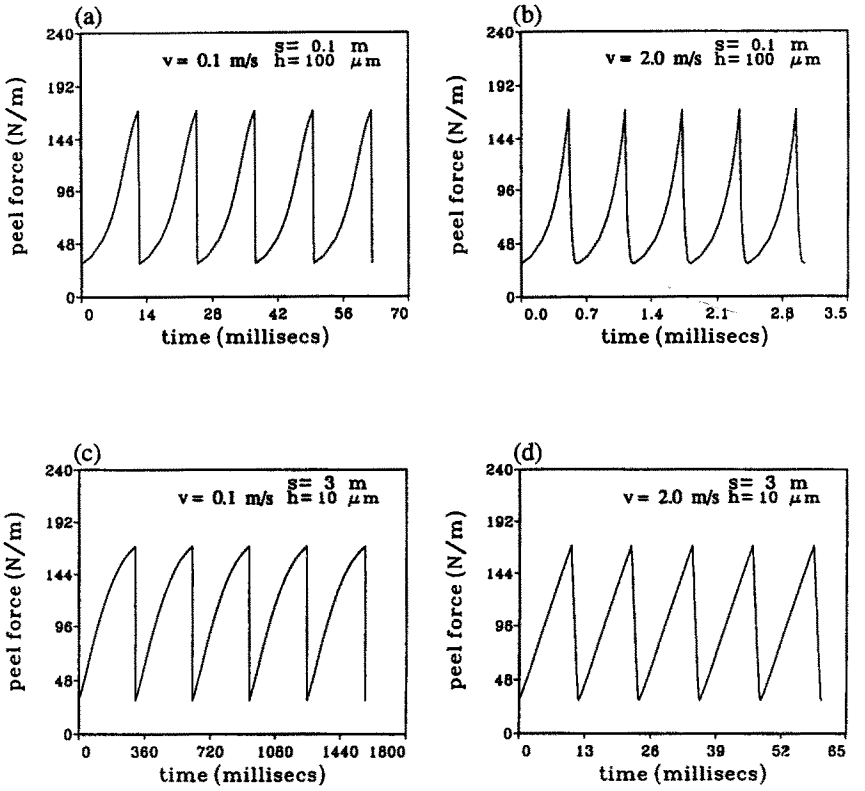

Fig. 8. Plots of peel force P vs time; (a) and (b) are for bending-dominant low-speed and high-speed peeling respectively, and (c) and (d) for stretching-dominant low-speed and high-speed peeling, respectively.

peeling speed. The peeled length, which is the length of the film peeled from the substrate, is also plotted with respect to time in Figs 10(a), (b), (c) and (d) in the same displaying order as in Figs 8 and 9. From these figures it is seen that for all cases most of the peeling occurs in the stage of high crack-growth rate, although less time is spent in this range. Especially at high peeling speed, almost all of the peeling occurs in the high crack-growth rate range. Therefore, the stick–slip phenomenon is more prominent at high peeling speeds.

4. DISCUSSION

In the previous sections we have provided the framework for the analysis of stick–slip crack growth caused by the interaction between the elastic deformation of the film and the variation of the rate-dependent fracture toughness in the peeling process. Now we will discuss the limitations of the analysis, and propose future improvements.

One of the assumptions we have made is that the film deforms elastically during the peeling process. This assumption is valid when the quantity $6EP/\sigma_y^2 h$ is less than one, where σ_y is the yield stress of the film. The scotch-tape peel test reported by Maugis and Barquins (1987) marginally satisfies the condition. A slight amount of plastic deformation occurred in the scotch-tape film. However, considerable amounts of plastic deformation accompanied the stick–slip peeling in the peel test of Kim and Kim (1989) for copper films on a silicon substrate. A typical trend in the stick–slip process during plastic peeling is that the amplitude of the peel-force fluctuation depends on the thickness of the film; the thinner the film the larger the amplitude. On the other hand, in elastic peeling the amplitude of the peel force fluctuation is independent of the thickness. Previous analysis by Kim and Aravas (1988) showed that the degree of plastic deformation increases as the film becomes thinner. It has also been shown that plasticity plays the role of an amplifier in the relationship between

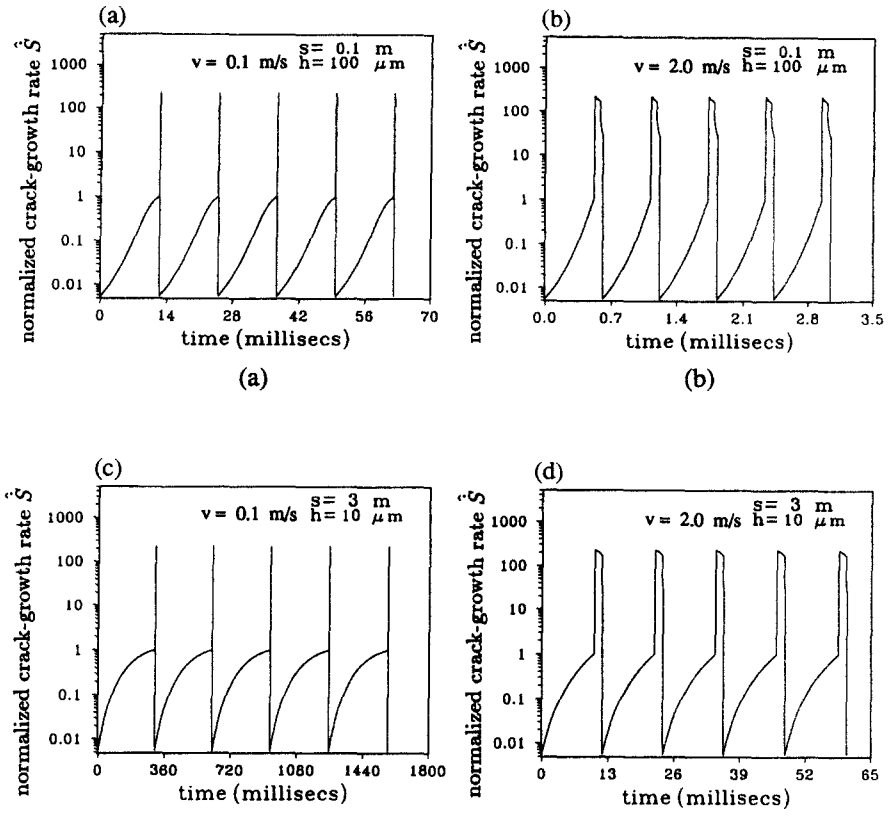

Fig. 9. Plots of normalized crack-growth rate $\hat{S}$ vs time; (a) and (b) are for bending-dominant low-speed and high-speed peeling respectively, and (c) and (d) for stretching-dominant low-speed and high-speed peeling, respectively.

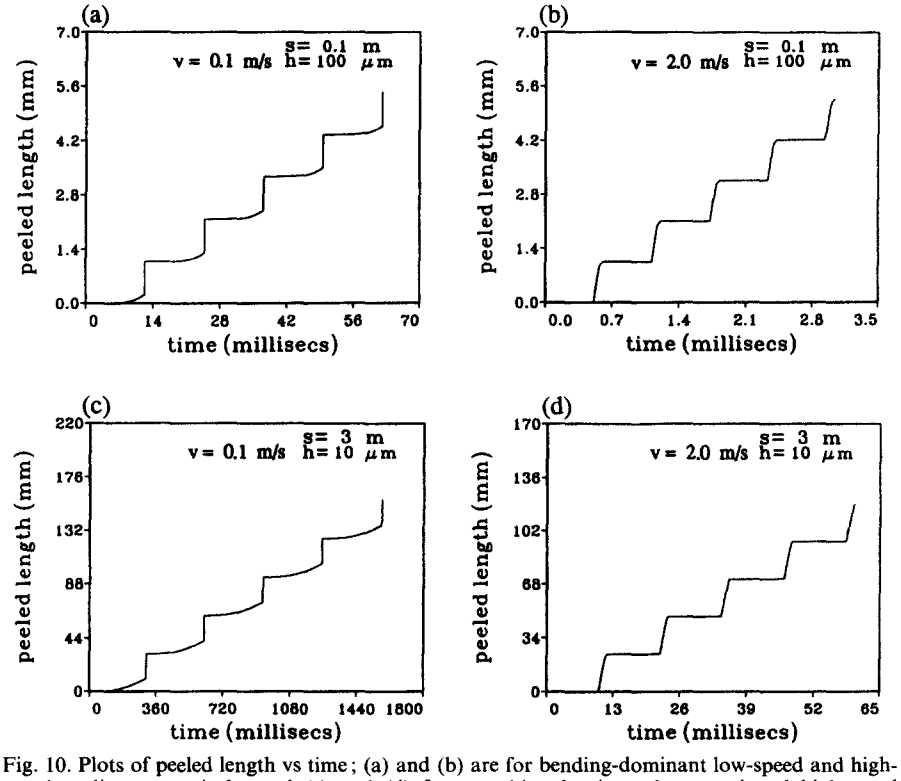

Fig. 10. Plots of peeled length vs time; (a) and (b) are for bending-dominant low-speed and high-speed peeling respectively, and (c) and (d) for stretching-dominant low-speed and high-speed peeling, respectively.

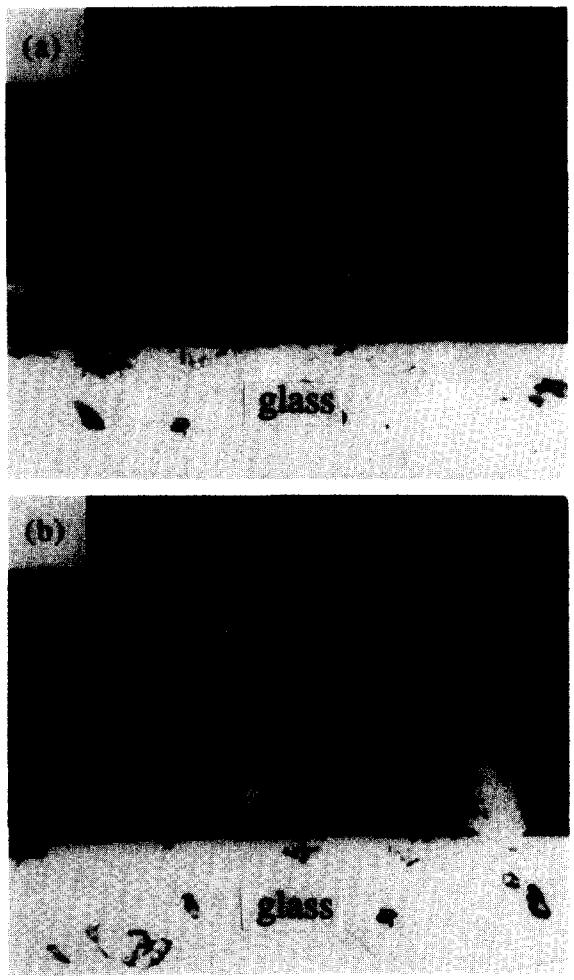

Fig. 11. Photographs of the cohesive zone at the crack tip in the scotch-tape peel test: (a) in the middle of stationary loading, (b) at onset of crack growth. Thickness of the tape is 50 μm.

the interface toughness and the peel force. Those analytic results agree qualitatively with the experimental observations. In the plastic peeling of Kim and Kim (1988), it is observed that the stick–slip frequency, for a given speed of peeling, also depends on the thickness of the film; the thicker the film the higher the frequency. The elastic analysis in this paper shows that the frequency is proportional to the thickness of the film for a stretching-dominant elastic peeling, while it is proportional to $1/h^{3/2}$ for a bending-dominant elastic peeling. For the case of a plastic peeling we speculate that the film curls as it is peeled off, and the curled film acts as a stretching spring during the peeling process. The stick–slip crack growth in plastic peeling still needs proper modeling, which will require tracing loading and unloading cycles of plasticity in the film. The inclusion of the effects of plasticity may result in a completely different mechanism producing the stick–slip process; a cycle of crack blunting, propagation and arrest may produce a rate-independent stick–slip phenomenon for a crack-growth-rate independent interface toughness. The effect of viscoelastic and viscoplastic deformation of the film on the stick–slip phenomenon may also have to be considered in future studies.

Another assumption we have employed in the analysis is that the fracture-process-zone size is small, and the fracture toughness is well defined. However the fracture-process-zone size may not be small compared to the thickness of the film for a scotch-tape peel test. In order to examine the peeling process in detail, we took microscopic photographs of the fracture process zone while a scotch tape (Scotch 3M 810) was peeling from a glass substrate. A video camera with a microscopic lens was used to record several images of the fracture process zone during the test. Figures 11(a) and (b) show side-view photographs taken at different times when the scotch tape was peeled at a low speed. The first photograph shows that an extensive cohesive zone formed at the crack tip before the interface crack propagated. Initially, the adhesive deformed more uniformly in the cohesive zone as shown in Fig. 11(a). As the peel force increased, the adhesive ruptured into clusters of fibrils as seen in Fig. 11(b). These photographs show that the cohesive zone size and the crack opening displacement are both much larger than the film thickness. In this case, the coupling of the film deformation and the adheisve deformation must be considered, and the influence of this cohesive zone on the peel analysis cannot be neglected.

Another factor that must be considered is the inertia effect on the stick–slip process. The quasi-static analysis predicts that, at the fastest stick–slip peeling speed, the frequency of the stick–slip process in a scotch tape peeling can attain 1 kHz for the film of 1 m detached length and 40 μm thickness. During the 1 m's period of the stick–slip cycle the tensile wave can only make a single round trip in the detached film. Therefore the validity of the quasistatic energy balance equation and the equation of static equilibrium employed in the analysis is questionable. For such high speed and high frequency stick–slip peeling we must consider the effect of film inertia in the analysis. Experiments show that the roller peeling produces even higher stick–slip frequencies than those predicted by the analysis of 90° peeling. In addition, the stick–slip process in the roller peel test sometimes exhibits chaotic fluctuations. For the analysis of crack growth in the roller peel test the kinetic energy of the roller must be included in the energy balance equation, and the variation of the peel angle during the peeling process must be considered in the momentum balance equations. Then the energy release rate in the roller peel test becomes a function of the crack-growth rate for given speed of peeling, peel angle, and angular speed of the roller (Tsai and Kim, 1993). As a consequence, the jump of crack-growth rate in the roller peel test, at the instant of instability, is much different from that in the 90° L peel test. In other words, the roller-peel stick–slip trajectory on the $(G, \dot{q})$ plane is much different from the limit cycle of the 90° L peel test. The roller-peel stick–slip can make much higher frequency, and the amplitude of the roller peel force fluctuation varies as a function of peeling speed.

5. CONCLUSION

Using a slender-elastic-beam theory and an energy-based criterion for crack growth, the equation of quasi-static crack growth, eqn (20), has been derived for 90° peeling of thin films. The crack-growth equation has been analysed for the stick–slip peeling process. The

analysis shows that the energy release rate, G, and the crack-growth rate, $\dot{q}$, form a limit cycle in the $(G, \dot{q})$ plane for the stick–slip 90° peeling. The analysis also revealed that there are two types of elastic peeling: the bending and stretching-dominant peelings. If the quantity $11.8\bar{P}^{3/2}\bar{S}$ is much greater than one, the peeling is stretching dominant. However, if it is much less than one, bending effects dominate. The variation of peel force during stick–slip peeling is different for stretching- and bending-dominant peelings. Furthermore, the dependence of stick–slip frequency on the thickness, the stiffness and the length of the free film is completely different for these two types of peelings [see eqn (24)]. In future studies the effects of the inertia and the plastic deformation of the free film can be included in the framework of the analysis provided in this paper.

Acknowledgements—This work was supported by the solid mechanics program of the U.S. Office of Naval Research (Contract No. N00014-90-J-1295) and solid and geomechanics program of the U.S. National Science Foundation (Contract No. NSF-MSS-9017933).

REFERENCES

Aubrey, D. W., Welding, G. N. and Wong, T. (1969). Failure mechanism in peeling of pressure-sensitive adhesive tape. *J. Appl. Polymer Sci.* **13,** 2193–2207.

Cook, R. F., Thouless, M. D., Clarke, D. R. and Kroll, M. C. (1989). Stick–slip during fiber pull-out. *Scripta Metall.* **23,** 1725–1730.

Dieterich, J. H. (1979). Modeling of rock friction—1. Experimental results and constitutive equations. *J. Geophys. Res.* **84**(B5), 2161–2168.

Gardon, J. L. (1963). Peel adhesion—I. Some phenomenological aspects of the test. *J. Appl. Polymer Sci.* **7,** 625–641.

Greensmith, H. W. and Thomas, A. G. (1955). Rupture of rubber—III. Determination of tear properties. *J. Polymer Sci.* **18,** 189–200.

Kendall, K. (1975). Thin-film peeling, the elastic term. *J. Phys. D: Appl. Phys.* **8,** 1449–1452.

Kim, K.-S. and Aravas, N. (1988). Elastoplastic analysis of the peel test. *Int. J. Solids Structures* **24,** 417–435.

Kim, K.-S. and Kim, J. (1988). Elasto-plastic analysis of the peel test for thin film adhesion. *J. Engng Mater. Tech.* **110,** 266–273.

Kim, J., Kim, K.-S. and Kim, Y. H. (1989). Mechanical effects in peel adhesion test. *J. Adhesion Sci. Technol.* **3**(3), 175–187.

Kinloch, A. J. and Yuen, M. L. (1989). The mechanical behavior of polymer-copper laminates. Part 1: Locus of failure studies. *J. Mater. Sci.* **24,** 2183–2190.

Liechti, K. M. and Chai, Y.-S. (1992). Asymmetric shielding in interfacial fracture under in-plane shear. *J. Appl. Mech.* **59,** 295–304.

Maugis, D. and Barquins, M. (1987). Stick–slip and peeling of adhesive tapes. In *Adhesion* (Edited by K. W. Allen), Vol. 12, pp. 205–222. Elsevier Applied Science, London.

Selby, K. and Miller, L. E. (1975). Fracture toughness and mechanical behavior of an epoxy resin. *J. Mater. Sci.* **10,** 12–24.

Spanoudakis, J. and Young, R. J. (1980). Crack propagation in a glass particle-filled epoxy resin—Part I. Effect of particle volume fraction and size. *J. Mater. Sci.* **19,** 473–486.

Thompson, P. A. and Robbins, M. O. (1990). Origin of stick–slip motion in boundary lubrication. *Science* **250,** 792–794.

Thouless, M. D. and Jensen, H. M. (1992). Elastic fracture mechanics of the peel-test geometry. *J. Adhesion* **38,** 185–197.

Tsai, K.-H. and Kim, K.-S. (1991). A study of stick–slip behavior in interface friction using optical fiber pull-out experiment. Presented at SPIE's Annual Meeting.

Tsai, K.-H. and Kim, K.-S. (1993). Stick–slip in the thin film peel test—Part II. The roller peel test. *Int. J. Solids Structures* (submitted).

Webb, T. W. and Aifantis, E. C. (1989). Stick–slip peeling. Presented at the Winter Annual Meeting.

Wu, T. W. (1991). Microscratch and load relaxation tests for ultra-thin films. *J. Mater. Res.* **6**(2), 407–426.